Sensitivity to Large-Scale Environmental Fields of the Relaxed Arakawa–Schubert Parameterization in the NASA GEOS-1 GCM

YAN YANG

Supercomputer Computations Research Institute, The Florida State University, Tallahassee, Florida

I. M. NAVON

Department of Mathematics and Supercomputer Computations Research Institute, The Florida State University, Tallahassee, Florida

RICARDO TODLING

NASA/DAO, and General Sciences Corporation, Greenbelt, Maryland

WEIYU YANG

Environmental Modeling Center, NCEP and UCAR, Camp Springs, Maryland

(Manuscript received 26 June 1998, in final form 5 November 1998)

ABSTRACT

An adjoint sensitivity analysis of the relaxed Arakawa–Schubert scheme in the National Aeronautics and Space Administration GEOS-1 GCM with respect to perturbations in large-scale environmental fields was conducted. The response functions were defined as measures of the strength of convective cloud precipitation, the cloud-induced heating and drying (moistening) in both the instantaneous and time-integrated sense. The roles of different variables in producing variations on the response functions were evaluated and the most sensitive vertical levels of the perturbations were identified with the gradient provided by the adjoint model.

It was found that the potential temperature perturbations had significant impact on all the response functionals analyzed, especially on the convective precipitation. The perturbations at subcloud layers and at midtroposphere from 500 to 600 hPa were found to be the most influential. The impact from the moisture fields was most significant on cloud heating and drying effects and the strongest influence came from the subcloud layers. The moisture perturbations at midtroposphere also significantly influenced the cloud drying (moistening) effect. On the other hand, the cloud-induced heating and drying at levels between 400 and 600 hPa felt the strongest impact from perturbations in large-scale fields. The influence of the perturbations in the wind field was weaker but still provided reasonable sensitivity patterns. The time-integrated and instantaneous sensitivities for the same response differ only in magnitude but not in the general distributions.

The impact of large-scale condensation and reevaporation on the sensitivity was also evaluated. Their effect was significant at the midtropospheric level and they enhanced the model sensitivity to perturbations in temperature and moisture fields.

The sensitivity analysis results obtained indicated that accurate gridscale vertical profile of temperature and moisture, especially at subcloud layers and midtroposphere between 500 and 600 hPa were essential for the accurate evaluation of the cumulus cloud effects. The implications of the results of this work for variational data assimilation were also discussed.

1. Introduction

The heating and moistening (drying) induced by convective clouds play an important role in the energy balance and water budget in the global atmosphere, therefore the representation of the effects of convective clouds is recognized as a key process in numerical weather prediction for timescales ranging from short-term forecasting to seasonal prediction and climate simulation. Moreover, an accurate parameterization of subgrid moisture processes in a general circulation model (GCM) is essential to fully assimilate such observational data as precipitation, cloudiness, and outgoing radiation, which are closely related to moisture and convection.

The Goddard Earth Observing System-1 (GEOS-1) GCM was developed by the Data Assimilation Office (DAO) at the National Aeronautics and Space Admin-

Corresponding author address: Prof I. M. Navon, Department of Mathematics, Supercomputer Computations Research Institute, The Florida State University, Tallahassee, FL 32306-4052.
E-mail: navon@scri.fsu.edu

istration Goddard Space Flight Center Goddard Laboratory for Atmospheres in collaboration with the Climate and Radiation Branch [for details please refer to Takacs et al. (1994)]. It is used in conjunction with an analysis scheme to produce a multiyear global atmospheric dataset for climate research (Schubert et al. 1993). It has also been used to produce multiple 10-yr climate simulations.

There are four physics packages in the GEOS-1 GCM, namely, the relaxed Arakawa–Schubert (RAS) parameterization and large-scale condensation schemes, the shortwave radiation and longwave radiation schemes, and the turbulence parameterization scheme, respectively. Among them the moisture processes play an essential role in the quality of the products of the data assimilation system (DAS). The RAS parameterization scheme (Moorthi and Suarez 1992) is the central part of the moisture processes.

The RAS scheme is a parameterization of the subgrid cumulus convection in terms of the large-scale fields. It computes the cloud-induced variations in potential temperature θ and moisture q as well as convective precipitation according to large-scale conditions in θ and q. The output impacts on the large-scale fields and in turn the modified environmental conditions influence the cloud activities. To improve the model forecast and the quality of data assimilation products, a thorough understanding of the interactions between large-scale fields and convective clouds in the model and an evaluation of the performance of the parameterization scheme in terms of its sensitivity to the large-scale environmental fields are indispensable prerequisites. The present work represents an effort toward this goal.

In a sensitivity study a gradient of a certain measure of model output (response function) is calculated with respect to perturbations in the model input variables and parameters. There are two approaches to calculate the gradient. One consists of the conventional forward sensitivity analysis, also called the perturbation method. In this algorithm, a series of experiments are carried out, each with one parameter or one state variable at one grid point being perturbed, then the variations in the response function produced by each of them are compared. Obviously, for large dimensional systems in question, this approach is computationally limited.

The other approach is the adjoint (backward) sensitivity analysis [Cacuci (1981a,b); see Cacuci (1988) for a review]. It provides an efficient way to calculate the gradient by a single integration of the adjoint model and is particularly suitable for the problems in atmospheric and oceanic models with large dimensions and relatively few responses. It has been successfully applied to a wide range of sensitivity problems, for example, the sensitivity to model parameters by Hall et al. (1982), Hall (1986), Rinne and Järvinnen (1993); the sensitivity of blocking processes by Zou et al. (1993); and the sensitivity of forecast aspects to initial conditions by Rabier et al. (1992, 1996). It also has been used in parameter estimation (Navon 1998). Another related work is that of Fillion and Errico (1997), in which some basic aspects related to incorporating moist convective processes in a variational data assimilation framework are addressed.

In the present work an adjoint sensitivity study is carried out to evaluate the impact of gridscale perturbations on RAS output both qualitatively and quantitatively. The following issues are addressed:

- examining the spatial variation of the sensitivity and identifying the vertical levels where the perturbations have the largest impact on RAS output;
- evaluating the relative importance of the perturbations in the temperature, moisture, and wind fields of the surrounding air in changing the outputs of the RAS scheme; and
- discussing the feedback between the convective clouds and the large-scale fields.

The outline of this article is as follows. In section 2, we describe the theory and algorithm of adjoint sensitivity. Section 3 consists of a brief description of the RAS scheme in the GEOS-1 GCM. Section 4 presents the results of the sensitivity analyses. Summary, conclusions, and the implications of this work for further research are provided in section 5.

2. Adjoint sensitivity method

In sensitivity analysis, we first define a response function R, which is a measure of the forecast aspects we are interested in. Here we consider only the functional type of response, that is, R is a real scalar:

$$R = R(\mathbf{x}),$$

where $\mathbf{x}$ is the vector consisting of all the model state variables over all the model grid points. We aim at evaluating the sensitivity of the change of R with respect to changes in $\mathbf{x}$. Specifically, we are concerned with the impact of small changes in the surrounding air on the output of the RAS scheme, since these outputs will in turn affect the large-scale environmental fields, which are directly relevant to the model forecast.

Let $\mathbf{y} = \mathbf{A}(\mathbf{x}, t)$ represent the output vector of the RAS scheme, where $\mathbf{x}$ is the vector consisting of the large-scale environmental fields that are inputs of RAS scheme, t is time, and $\mathbf{A}$ represents the nonlinear RAS operator. The following three general types of response functionals are considered:

$$R_1 = \langle \mathbf{y}, \mathbf{y} \rangle_{\mathbf{S}} = \mathbf{y}^T \mathbf{S} \mathbf{y}, \tag{1}$$

where $\langle \cdot , \cdot \rangle_{\mathbf{S}}$ stands for the inner product between two vectors weighted by a real, symmetric matrix $\mathbf{S}$ specified according to the field of interest, $(\cdot)^T$ stands for the transpose operation,

$$R_2 = \langle \mathbf{w}, \mathbf{y} \rangle = \mathbf{w}^T \mathbf{y}, \tag{2}$$

where $\mathbf{w}$ is a specified weighting vector and $\langle \cdot , \cdot \rangle$ is a

normal Euclidean inner product; the above two functionals are viewed as instantaneous responses, that is, they refer to a given time, which is the same as that of the input variables. Finally, we also define a time-integrated response as

$$R_3 = \int_{t_0}^{t_N} \langle \mathbf{y}, \mathbf{y} \rangle_{\mathbf{S}}\, dt = \int_{t_0}^{t_N} \mathbf{y}^T \mathbf{S}\mathbf{y}\, dt. \tag{3}$$

a. Instantaneous sensitivity

To determine the impact of small perturbations in the surrounding air on R, we need to evaluate the gradient of R with respect to the input $\mathbf{x}$. Using a Taylor series expansion and retaining only the first-order approximation, a small perturbation $\delta\mathbf{x}$ on the state vector causes a change δR_1 in the response function that can be calculated by

$$\delta R_1 = 2\langle \mathbf{y}, \delta\mathbf{y} \rangle_{\mathbf{S}} = 2\left\langle \mathbf{y}, \frac{\partial \mathbf{A}(\mathbf{x}, t)}{\partial \mathbf{x}} \delta\mathbf{x} \right\rangle_{\mathbf{S}} = 2\mathbf{y}^T \mathbf{S} \left[\frac{\partial \mathbf{A}(\mathbf{x}, t)}{\partial \mathbf{x}} \delta\mathbf{x} \right]$$

$$= 2\left\{ \left[\frac{\partial \mathbf{A}(\mathbf{x}, t)}{\partial \mathbf{x}} \right]^T \mathbf{S}^T \mathbf{y} \right\}^T \delta\mathbf{x} = 2\left\langle \left[\frac{\partial \mathbf{A}(\mathbf{x}, t)}{\partial \mathbf{x}} \right]^T \mathbf{S}^T \mathbf{y}, \delta\mathbf{x} \right\rangle, \tag{4}$$

where $\partial \mathbf{A}(\mathbf{x}, t)/\partial \mathbf{x}$ is the Jacobian representing the tangent-linear operator of the RAS scheme. The adjoint with respect to the normal Euclidean inner product is simply its transpose $[\partial \mathbf{A}(\mathbf{x}, t)/\partial \mathbf{x}]^T$.

From (4) we can see that the gradient of R_1 with respect to $\mathbf{x}$ is

$$\nabla_{\mathbf{x}} R_1 = 2\left[\frac{\partial \mathbf{A}(\mathbf{x}, t)}{\partial \mathbf{x}} \right]^T \mathbf{S}^T \mathbf{y} = 2\left[\frac{\partial \mathbf{A}(\mathbf{x}, t)}{\partial \mathbf{x}} \right]^T \mathbf{S}\mathbf{y}. \tag{5}$$

In practice, this can be obtained by first running the original RAS with a prescribed large-scale field at a certain time t to obtain $\mathbf{y} = \mathbf{A}(\mathbf{x}, t)$, then apply the operator $\mathbf{S}$, which here is a simple scaling operation, and finally take the result as the input to the adjoint of RAS. The output of the adjoint of RAS yields the gradient vector. The component of the vector corresponding to each of the variables is the gradient of R_1 with respect to that particular variable.

For the response R_2, similar reasoning as above leads to

$$\nabla_{\mathbf{x}} R_2 = \left[\frac{\partial \mathbf{A}(\mathbf{x}, t)}{\partial \mathbf{x}} \right]^T \mathbf{w}, \tag{6}$$

where now the input to the adjoint of RAS is the weighting vector $\mathbf{w}$ instead of $\mathbf{S}\mathbf{y}$ for R_1.

b. Time-integrated sensitivity

The perturbation of the response R_3 is derived as above and can be expressed as

$$\delta R_3 = 2\int_{t_0}^{t_N} \left\langle \left[\frac{\partial \mathbf{A}(\mathbf{x}, t)}{\partial \mathbf{x}} \right]^T \mathbf{S}^T \mathbf{y}, \delta\mathbf{x} \right\rangle dt. \tag{7}$$

We need to evaluate the gradient of R_3 with respect to the initial perturbations $\delta\mathbf{x}_0 = \delta\mathbf{x}|_{t=t_0}$. Recall that a small perturbation $\delta\mathbf{x}(t)$ can be related to $\delta\mathbf{x}_0$ through the resolvent $\mathcal{L}(t, t_0)$ of the tangent-linear model of the GCM:

$$\delta\mathbf{x} = \mathcal{L}(t, t_0)\delta\mathbf{x}_0. \tag{8}$$

Defining $\mathcal{L}^*(t_0, t)$ as the adjoint of $\mathcal{L}(t, t_0)$, δR_3 may be written as

$$\delta R_3 = \left\langle 2\int_{t_0}^{t_N} \left\{ \mathcal{L}^*(t_0, t) \left[\frac{\partial \mathbf{A}(\mathbf{x}, t)}{\partial \mathbf{x}} \right]^T \mathbf{S}^T \mathbf{y} \right\} dt, \delta\mathbf{x}_0 \right\rangle. \tag{9}$$

Therefore the gradient of R_3 with respect to initial perturbation is given by

$$\nabla_{\mathbf{x}_0} R_3 = 2\int_{t_0}^{t_N} \left\{ \mathcal{L}^*(t_0, t) \left[\frac{\partial \mathbf{A}(\mathbf{x}, t)}{\partial \mathbf{x}} \right]^T \mathbf{S}^T \mathbf{y} \right\} dt. \tag{10}$$

By definition, in areas with large gradient, a perturbation $\delta\mathbf{x}_0$ would create a larger impact on R_3 than the same perturbation in areas with small gradient. Thus the 3D distribution of this gradient provides the sensitivity pattern of R_3 to $\mathbf{x}_0$. Also this gradient yields the optimal initial perturbation pattern in the sense that for all the initial perturbations with unit norm $\|\mathbf{x}_0\|$, the one with the same spatial distribution as $\nabla_{\mathbf{x}_0} R_3$, that is, parallel to $\nabla_{\mathbf{x}_0} R_3$ in phase space, imposes the largest changes in R_3. The same argument applies to the gradients of R_1 and R_2. In the present paper we use the terms gradient and sensitivity interchangeably.

In practice, the algorithm to calculate the gradient vector (10) is as follows.

1) Integrate the GCM from time $t = t_0$ to $t = t_N$, saving the environmental fields as well as the RAS output [$\mathbf{y}$ in (10)] at times t_n, for $n = 0, 1, 2, \ldots, N$.
2) At each time t_n, use the stored trajectory of RAS output [$\mathbf{y} = \mathbf{A}(\mathbf{x}, t)$] and the adjoint RAS to calculate (5), the gradient with respect to instantaneous perturbations of the large-scale fields at each time t_n.
3) Finally, integrate the adjoint of the GCM backward in time from t_N to t_0, with the result of step 2 at t_N as the initial condition. Since $\mathcal{L}^*$ is linear, the result of step 2 is added to the corresponding environmental fields of the adjoint GCM at each t_n. The result at t_0 is $\nabla_{\mathbf{x}_0} R_3$ in (10).

Note that while (5) provides the sensitivity of the response with respect to instantaneous perturbation in the surrounding air, the integration of the adjoint of the GCM yields the time evolution of sensitivity.

The merit of the adjoint method lies in that a single adjoint model integration yields the gradient of one response function to all the model variables at all model grid points. If instead we were to use the forward direct

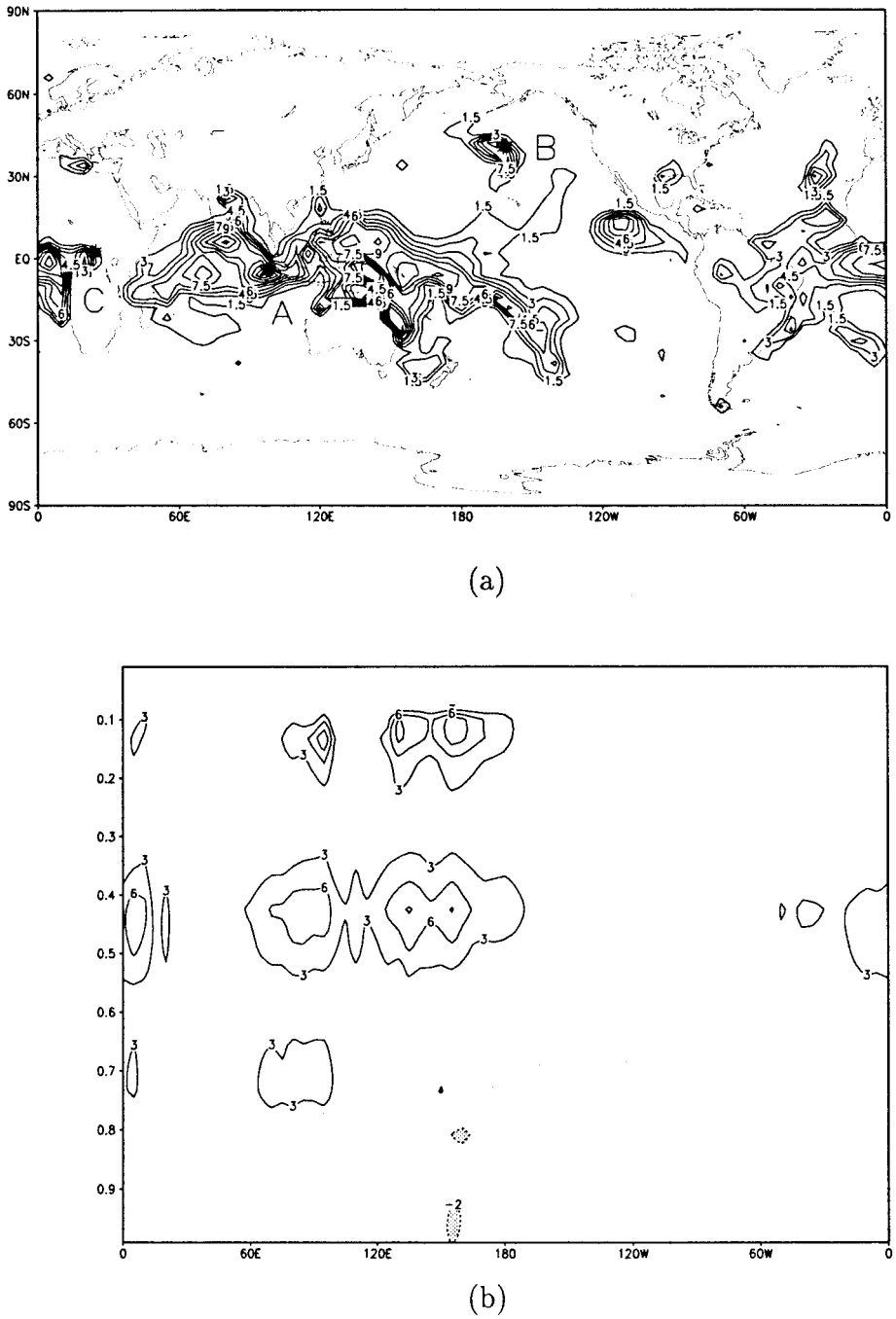

FIG. 1. Output from the RAS scheme at 0000 UTC 1 January 1985: (a) convective cloud precipitation (interval 1.5 mm day^{-1}); (b) cloud-induced rate of change in potential temperature, averaged between 10°S and 10°N (interval 2.0 $\times$ 10^{-4} K s^{-1}); (c) cloud-induced rate of change in moisture, averaged

sensitivity method, then to obtain the same information would require integrating the original model $N \times M$ times, where N is the number of variables and M is the number of model grid points (on the order of 10^5). This is computationally prohibitive even with the most powerful computers available today.

In what follows **w** and **S** are chosen to define different response functionals in order to examine various aspects of RAS sensitivity.

3. The moisture package of the GEOS-1 GCM

The moisture package of the GEOS-1 GCM consists of three components: the RAS scheme, the large-scale

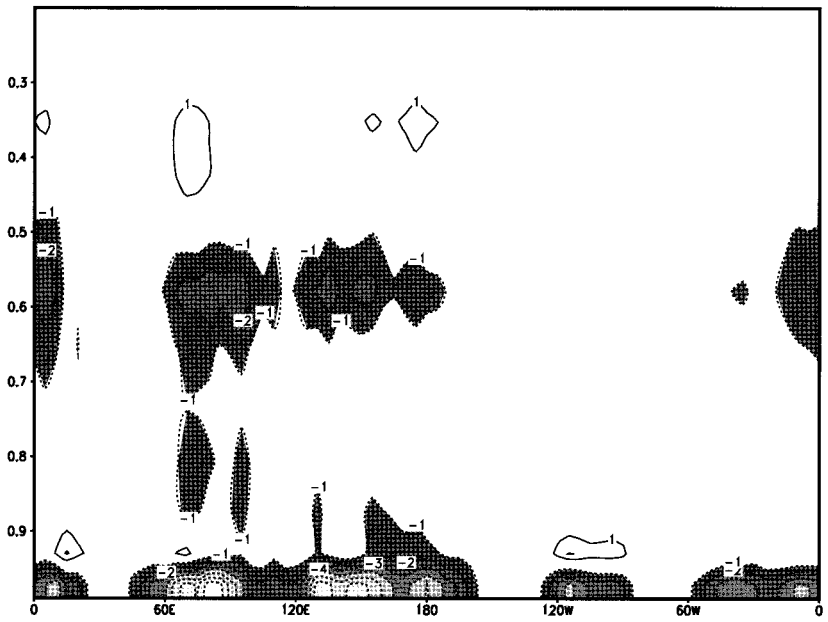

FIG. 1. (*Continued*) between 10°S and 10°N [interval 1.0×10^{-4} (g kg^{-1}) s^{-1}]. Shading indicates negative values. The ordinates in (b) and (c) are σ levels.

condensation, and reevaporation of the falling rain. The RAS scheme is a parameterization of the subgrid scale penetrative and shallow cumulus convection in terms of large-scale fields (Moorthi and Suarez 1992). It predicts mass fluxes from cloud types, which have different entrainment rates and levels of neutral buoyancy, depending on the properties of the large-scale environment. In this scheme, all clouds are assumed to have the same base but each cloud type is characterized by its detrainment level (cloud top). The normalized mass flux for each cloud type is a linear function of height. In the original Arakawa–Schubert scheme, the closure assumption is a balance between large-scale and gridscale effects on the cloud work function, which is a measure of efficiency of convection. In the RAS scheme, the major simplification is to relax the state toward equilibrium each time the parameterization is invoked, rather than requiring that the final state be balanced.

At each model time step, several different cloud types are treated sequentially. At any instant, each cloud interacts with only the current environment, which results from the effect of the previous cloud type in the sequence. In this way, the interactions between clouds are accounted for implicitly.

For the reevaporation, a Kessler-type scheme is employed (Sud and Molod 1988), adjusting the impact on the large-scale environment from RAS. Supersaturation or large-scale condensation is defined whenever the specific humidity in any grid box exceeds its supersaturation value. It also reevaporates during descent to partially saturated lower layers.

The adjoint of the adiabatic GCM and the moisture package were developed and documented in Yang and Navon (1996) and Yang et al. (1997). In the present study this package is the only physical process included in the adjoint model.

All the experiments were performed with a $5° \times 4°$ horizontal resolution and 20 vertical σ levels. The initial time is arbitrarily chosen at 0000 UTC 1 January 1985. The initial state is extracted from the DAO archived reanalysis data, which has the same resolution as above and includes five independent variables, namely the potential temperature, the zonal and meridional wind, the surface pressure, and the specific humidity. The time integration in evaluating (10) was carried out for 6 h.

To help understand the results of the sensitivity analysis study, we start by looking at the effect of convective cloud on the large-scale environment. Figure 1 displays some output from the RAS scheme at 0000 UTC 1 January 1985. Figure 1a shows the convective cloud precipitation, indicating that strong convective activity occurs over the low-latitude oceans, especially over the eastern Indian and the western Pacific Oceans as well as the Atlantic Ocean. The points A, B, and C are for later reference. In Fig. 1b the longitude–height distribution of the rate of convection-induced potential temperature change $\Delta\theta$, averaged between 10°S and 10°N, is shown (the ordinate is the vertical σ level). This indicates that convective clouds act as a heat source to the environmental air at all levels. The strongest heating occurs in the midtroposphere between $\sigma = 0.4$ and $\sigma = 0.5$ (between about 400 and 500 hPa),

above the Indian and western Pacific Oceans where the strong convective clouds occur. A very strong heating rate is also seen between levels $\sigma = 0.1$ and 0.2 (around 100–200 hPa). This is attributed to the way the heating rate is calculated. To be converted into an actual temperature change ΔT, $\Delta\theta$ should be multiplied by a factor $(p/p_0)^\kappa$, where p is the pressure and p_0 is a reference pressure, $\kappa = R/C_p$, where R is the gas constant and C_p is the specific heat at constant pressure. Therefore the heating at the higher levels is scaled down more than at the lower levels. Throughout this paper the heating rate is represented by $\Delta\theta$ rather than by ΔT. In Fig. 1c the rate of cloud-induced moisture change Δq is shown. Only the layers below $\sigma = 0.3$ are displayed. The convective cloud generally dries out the layers below 500 hPa, especially the subcloud layers and around 600 hPa, but only weakly moistens the upper layers. At midtroposphere, the layer with the strongest convective drying is lower than that with the strongest heating.

4. Sensitivity analysis results

The convective clouds impact upon the large-scale fields through the changes in potential temperature $\Delta\theta$ and moisture Δq. On the other hand, gridscale variations in vertical profile in the surrounding air influence convective activity. In this section we investigate the sensitivity of the RAS outputs to large-scale environmental fields, that is, the effect of small perturbations in the surrounding air on the RAS outputs.

All the gradients obtained using the adjoint model were subject to a gradient correctness test. For this purpose, the following function was calculated:

$$F(\beta) = \frac{R(\mathbf{x} + \beta\mathbf{h}_x) - R(\mathbf{x})}{\langle \nabla_x R, \beta\mathbf{h}_x \rangle}, \tag{11}$$

where $\mathbf{h}_x$ is a prescribed field of perturbations and β is a scaling factor controlling the magnitude of the perturbations. Here $\mathbf{h}_x$ is obtained by taking the difference between the result of a 6-h integration of the original GCM and the initial condition. Within several orders of magnitude of β, a unit value for $F(\beta)$ is obtained. As an example, Fig. 2 provides the result of the gradient check for R_1 response function. It indicates that the range of the validity of the adjoint sensitivity is from $\beta = 10^{-1}$ to $\beta = 10^{-9}$.

a. Instantaneous sensitivity

In this section we present the results from instantaneous sensitivity, that is, a response function of type R_2 in (2) is used with its gradient calculated following (6).

1) CONVECTIVE PRECIPITATION

The response function for this case is specifically defined as

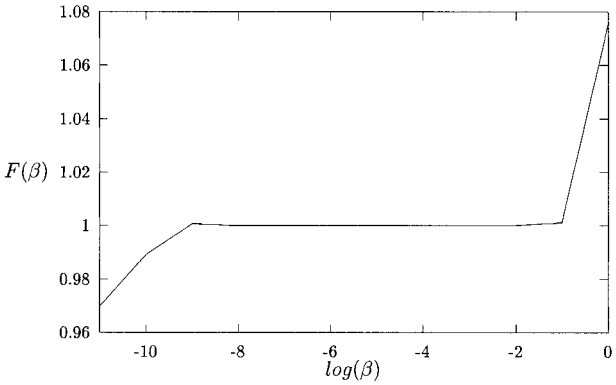

FIG. 2. Variation of $F(\beta)$ with respect to $\log(\beta)$, as indication of the validity of the linear approximation.

$$R_p = \sum_{\Omega} P_r,$$

where P_r is the convective cloud precipitation rate and Ω represents the low-latitude belt from 30°S to 30°N, where most of the precipitation occurs, as indicated in Fig. 1.

Figure 3a shows the longitude-vertical distribution of the sensitivity of precipitation to potential temperature, averaged between 10°S and 10°N. Positive sensitivity centers are observed below the cloud-base level (around 950 hPa). From this level above to the 250-hPa level, the gradient is largely negative in a relatively uniform way although a center is discerned at around 500 hPa over the western Pacific Ocean. Such a distribution means that if the surrounding air in the boundary layer gets warmer and the midtroposphere gets colder, there will be a stronger convective activity and stronger convective precipitation. For instance, if a positive perturbation of 1 K in temperature occurs at the point with the largest gradient in the subcloud layer, an increase of about 7 mm day^{-1} in the overall precipitation rate is induced. On the other hand, if this perturbation occurs at the point with the largest negative gradient, say around 500 hPa, it results in about 9 mm day^{-1} decrease in total convective rain. This is due to the fact that warming up at the lower level destabilizes the surrounding air and cooling down at the upper level strengthens the cloud buoyancy force, which is measured by the difference between the moisture static energy in the cloud plume and the environment, thus favoring convective cloud development.

The variation with height of the sensitivity of precipitation to moisture is displayed in Fig. 3b. Only the levels below 850 hPa show significant positive sensitivity with the largest gradient near the cloud-base level. This means that more moisture near this level favors convective activities and induces stronger convective precipitation. Specifically, if a 1 g kg^{-1} perturbation in the moisture field occurs at the largest gradient point at 950 hPa, it tends to induce about 3 mm day^{-1} increase in total cloud precipitation.

2) SENSITIVITY WITHIN A SINGLE COLUMN

From the former analysis, several representative grid points with high convective activity and high sensitivity were chosen for further analysis. The following three locations were used for single-column sensitivity in what follows:

point A: (6°S, 100°E),

point B: (42°N, 165°W),

point C: (2°S, 25°E).

Their locations are indicated in Fig. 1a by black dots and corresponding letters nearby.

Now the response functionals are defined as

$$R_\theta = \Delta\theta(i, j, k)/\Delta t, \tag{12}$$

and

$$R_q = \Delta q(i, j, k)/\Delta t, \tag{13}$$

where (i, j, k) indicates a particular horizontal grid point (i, j) at a particular vertical level k and Δt is the RAS time step. Since the RAS scheme is implemented columnwise, the output at a particular point at a certain level can be sensitive to all the other vertical levels at this point, but not to the surrounding grid points. In a single column, the gradients of R_θ and R_q to environmental θ and q constitute the four component blocks of a Jacobian matrix, which is given by

$$\begin{vmatrix} \nabla_\theta(R_\theta) & \nabla_q(R_\theta) \\ \nabla_\theta(R_q) & \nabla_q(R_q) \end{vmatrix}. \tag{14}$$

Figure 4 displays the four components of the Jacobian (14) at point A over the eastern Indian Ocean. The ordinate is the σ level corresponding to k in R_θ in (12) and (13), going from the surface upward, and is referred to as the response level. The abscissa consists of the σ levels of the surrounding air where perturbations occur and are referred to as the influential levels. For example, the large negative value at point (0.5, 0.45) in Fig. 4a provides the gradient of R_θ at point A at level $\sigma = 0.45$ (near 450 hPa) with respect to perturbations in θ at level $\sigma = 0.5$ (around 500 hPa).

From Figs. 4a–b one can see that for R_θ, the level around 450 hPa displays the largest sensitivity, with positive gradient to both θ and q in the subcloud layers, where a 1 K increase in θ leads to about 4 K day^{-1} increase in cloud heating at the 450-hPa level, whereas an additional 1 g kg^{-1} in the moisture content leads to about 8.7 K day^{-1} increase in heating at the 450-hPa level in terms of θ change. This impact is very significant. Furthermore, Fig. 4a shows a significant negative gradient with respect to θ near 500 hPa, where a 1 K decrease in θ leads to a 5.6 K day^{-1} increase in cloud heating rate at around 450 hPa. This implies a negative feedback between the θ perturbation in the environmental air and the cloud-induced heating at around 450 hPa.

The opposite impacts of perturbations occurring at 500 and 400 hPa on the convective heating can be explained by the fact that environmental heating is mainly accomplished by compensating downdrafts outside the clouds induced by the updrafts inside the clouds (Redelsperger and Guichard 1996). Lower environmental air temperature in the midtroposphere increases the difference of static energy between the cloud and the environment, thus increasing the buoyant force. This induces stronger updraft inside the cloud and downdraft outside it and thus stronger heating of the air column. On the other hand, if the layer around 400 hPa gets colder, the heating through subsidence at the 450-hPa level will be less effective. This explains the two opposite centers observed below and above 450 hPa in Fig. 4a. The implication is that in order to accurately parameterize the cloud effects, an accurate vertical profile of the surrounding air is an essential prerequisite.

For R_q, the most influential layer is the subcloud layer (Figs. 4c and 4d). The midlevel perturbation can also exert significant influence, however, only on the adjacent layers. The layer around 500–600 hPa is significantly influenced by the θ and q perturbations in the surrounding air at the same level as well as at subcloud levels. A raise of 1 K in temperature and 1 g kg^{-1} in moisture content at subcloud layer tends to enhance convection, leading to a stronger convective drying of about 7×10^{-3} and 5×10^{-3} g kg^{-1} day^{-1}, respectively, in the midtroposphere (note from Fig. 1c that Δq is negative at most of the vertical levels). On the other hand, occurrence of positive θ and negative q perturbations at midtroposphere around 600 hPa tends to suppress convective drying at the same level. Note the opposite effect of the q perturbations at $\sigma = 0.5$ (500 hPa) and $\sigma = 0.6$ (600 hPa) levels on the convective drying at 600 hPa. At around 600 hPa, the negative gradient implies that the feedback between the moisture perturbation and cloud drying effect is negative, whereas near 500 hPa, the feedback changes to positive. The behavior of point A is typical of model gridpoint locations over low-latitude oceans with strong deep convective clouds.

Now we turn our attention to point B over the midlatitude Pacific Ocean. Figure 5 shows the four components of the Jacobian at this point. Comparing Figs. 5a and 5b with Figs. 4a and 4b, respectively, one can see that for R_θ, the strongest response level is lowered to $\sigma = 0.5$ (around 500 hPa). This layer shows significant sensitivity to θ perturbations at the same level as well as to that at the levels below. For R_q, Figs. 5c and 5d show that the strongest response level is confined to below $\sigma = 0.8$. Negative θ and positive q perturbations between $\sigma = 0.8$ and $\sigma = 0.9$ (800–900 hPa) induce stronger convective drying. Also, the positive θ perturbation around $\sigma = 0.6$ level can lead to a suppression of convective drying at the layers lower than 850 hPa. This may be attributed to the reduced buoyancy force by higher environmental temperature.

The diagonal structure of the Jacobian, which is most

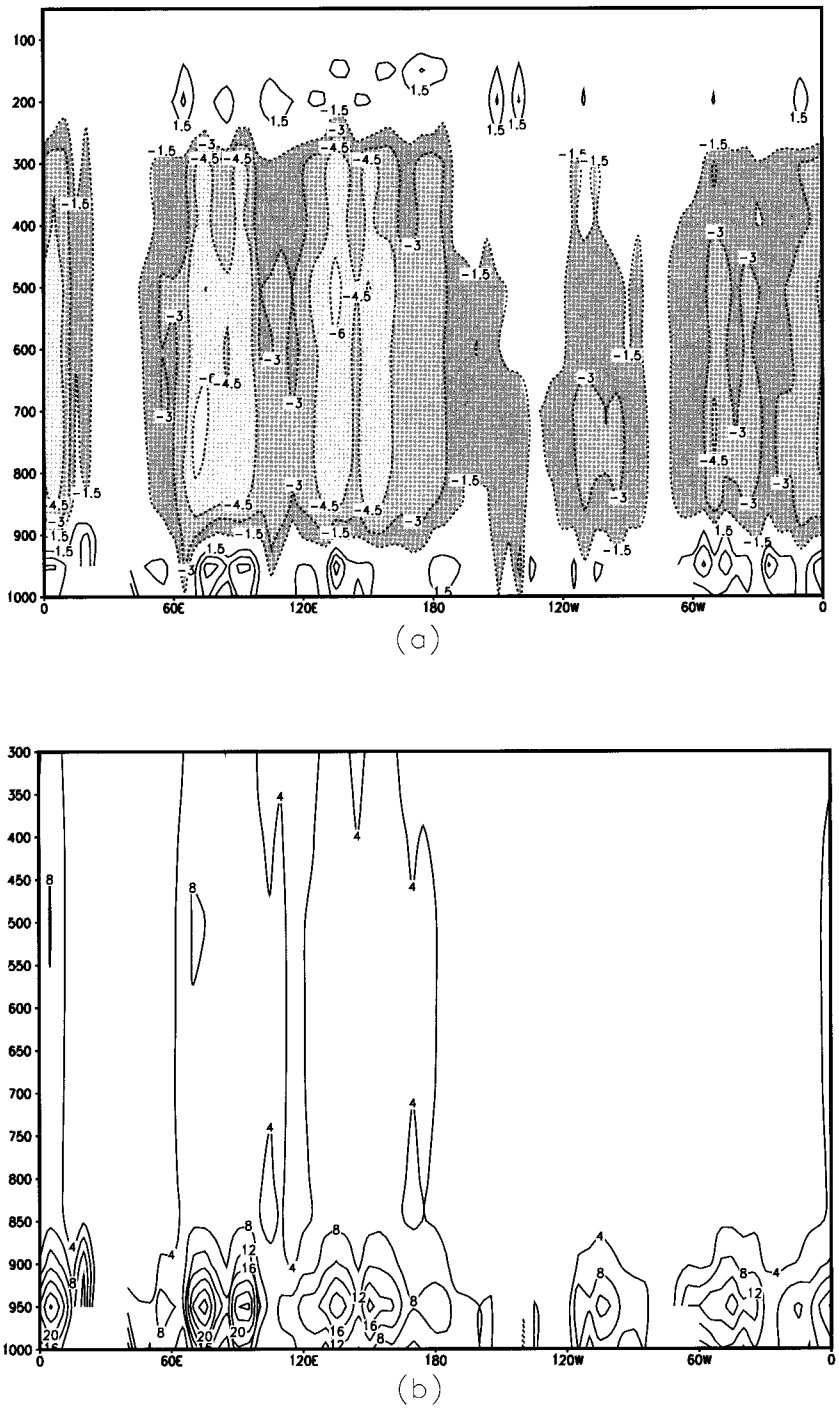

FIG. 3. Longitude–vertical distribution of the sensitivity of the RAS precipitation to perturbations in (a) the potential temperature field [interval 1.5, one unit corresponds to 1.4 (mm day^{-1}) K^{-1}], and (b) the moisture field {interval 4.0, one unit corresponds to 0.1 (mm day^{-1}) [g kg^{-1}]$^{-1}$}, averaged between 10°S and 10°N. The ordinates are in hPa.

evident in Fig. 5d, indicates the local effect of the perturbations on convective drying. The R_q at layers above 500 hPa shows little sensitivity to the θ and q perturbations at any level, probably since at this location the convective clouds cannot penetrate to very high levels due to the fact that the moisture content in the air column is lower than that at low latitudes.

Figure 6 displays the Jacobian at grid point C over the tropical African continent. For R_θ, the major difference between the points C and A is that now the

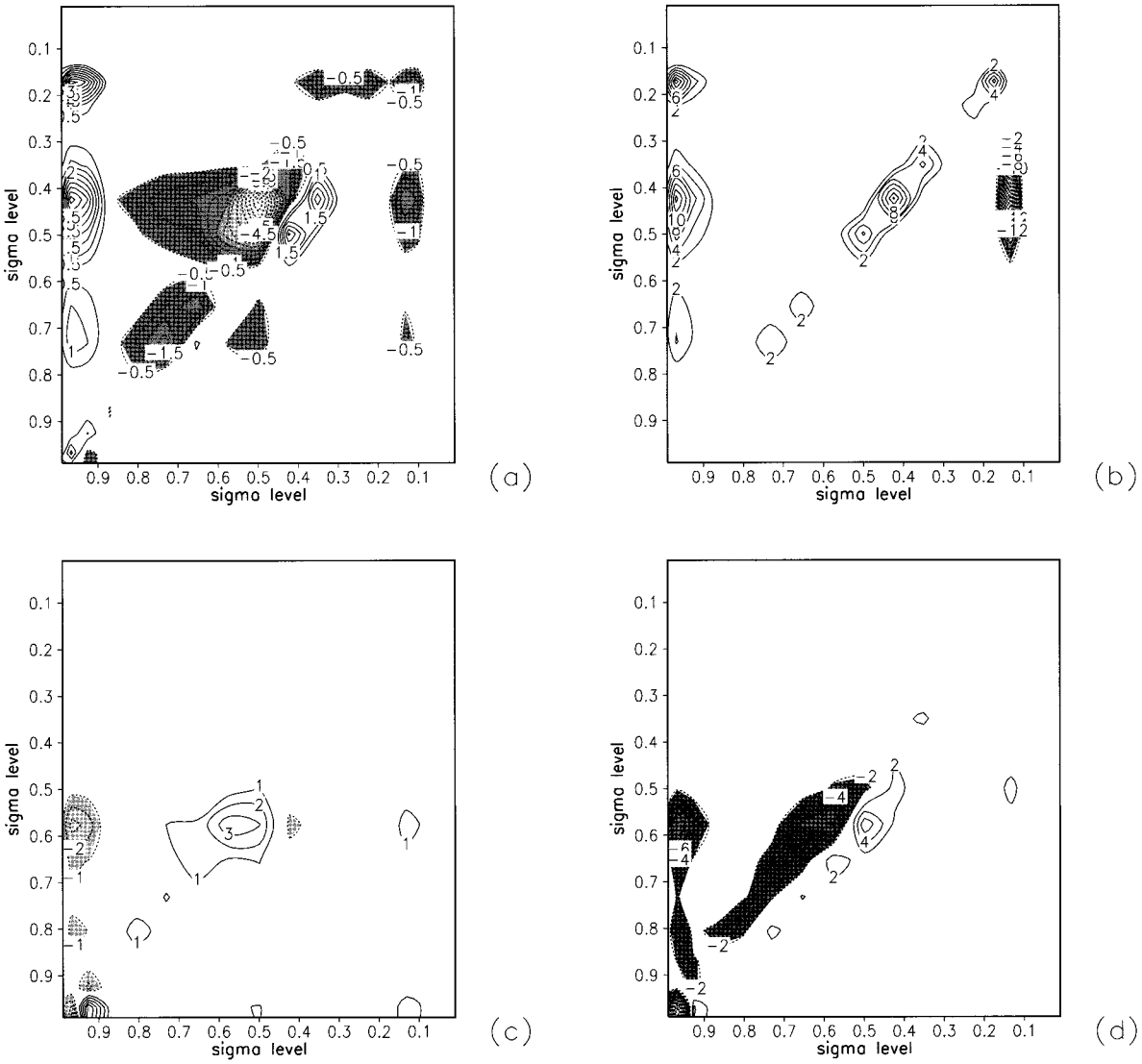

FIG. 4. The four blocks of the Jacobian at point (6°S, 100°E): (a) $\nabla_\theta(R_\theta)$, interval 0.5, one unit corresponds to 0.86 (K day^{-1}) K^{-1}; (b) $\nabla_q(R_\theta)$, interval 2.0, one unit corresponds to 0.62 (K day^{-1}) (g kg^{-1})$^{-1}$; (c) $\nabla_\theta(R_q)$, interval 1.0, one unit corresponds to 1.2×10^{-3} (g kg^{-1} day^{-1}) K^{-1}; and (d) $\nabla_q(R_q)$, interval 2.0, one unit corresponds to 0.86×10^{-3} (g kg^{-1} day^{-1}) (g kg^{-1})$^{-1}$.

sensitivity of midtroposphere R_θ to both θ and q disturbances is about an order of magnitude weaker (notice the difference in the contour intervals). Here the impact on convective heating from perturbations at mid- to upper troposphere is relatively more important than that from subcloud layers.

For R_q, Figs. 6c and 6d show a marked difference compared to locations A and B. Now both the significantly sensitive layer and the influential layer are confined to below 900 hPa (notice the different scales in the ordinate and abscissa between Figs. 6c,d and the corresponding figures for points A and B in Figs. 4 and 5). This is probably due to the presence of less moisture content in the air column and lower cloud top over land area than over the low-latitude oceans. However, Figs. 6c and 6d still display detailed sensitivity structures with respect to the temperature and moisture perturbations, that is, positive θ and q perturbations at the lowest model level and negative perturbations higher above (between 900 and 950 hPa) tend to destabilize the subcloud layers and strengthen convective drying. In fact at locations A and B such sensitivity structures at the lowest model levels are also observed. At the lowest model layers the points considered here depict strong negative feedback between q and the convective drying, whereas in the slightly higher layers, the feedback is positive.

From the analysis above for the three types of grid-point locations we can conclude that the perturbations in the subcloud layers can most significantly influence the convective activities at each of these locations. For cloud effects at midtroposphere, the influence from subcloud-layer disturbances may surpass that arising from

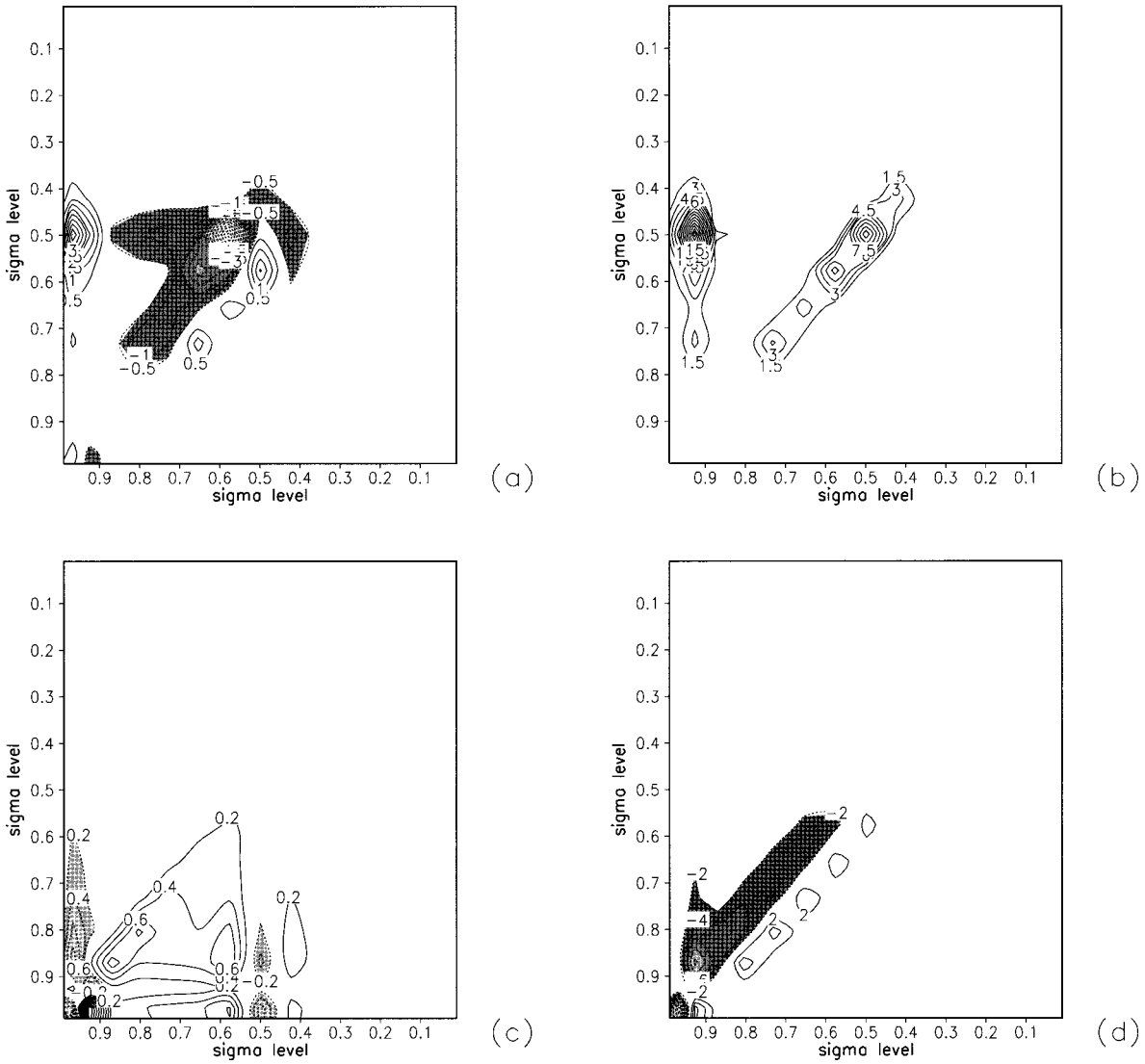

FIG. 5. Same as Fig. 4 but for point (42°N, 165°W): (a) $\nabla_\theta(R_\theta)$, interval 0.5; (b) $\nabla_q(R_\theta)$, interval 1.5; (c) $\nabla_\theta(R_q)$, interval 0.2; and (d) $\nabla_q(R_q)$, interval 2.0.

perturbations in the immediate surrounding air at the same level, especially for R_θ at grid points over the oceans. As to the response functions, the midtroposphere is the one most easily influenced. The variations in cloud heating and drying effects are larger at these levels than at other levels if forced by the same perturbation. Over land and high-latitude oceans, the moisture perturbation exhibits more localized effects, which are mostly confined to the lowest model levels, whereas over the low-latitude oceans with high sea surface temperature (SST) and stronger deep clouds, the impact of the boundary layer can be more readily transferred to higher levels.

Fillion and Errico (1997) discuss the distribution of the blocks of the Jacobian at a single gridpoint location with strong convection, for both the Kuo and the RAS schemes. For the RAS scheme, they use the direct perturbation method instead of adjoint sensitivity to generate the Jacobian. Similar to what we observed here, they point out the influence from the lowest model layers, but their results show a stronger upper-level diagonal structure, which indicates a more localized effect than ours. This difference between the results may be attributed to the choice of different time and geographic locations.

We can see that most of the layers display negative feedback between R_θ and the θ perturbation and between R_q and q perturbation. This suggests that perturbations in the surrounding air are suppressed by cloud activities. Therefore the cloud effect is by and large a stabilizing factor for large-scale perturbations. However, there are some vertical levels with positive feedback, to which more attention should be paid, since the interaction can

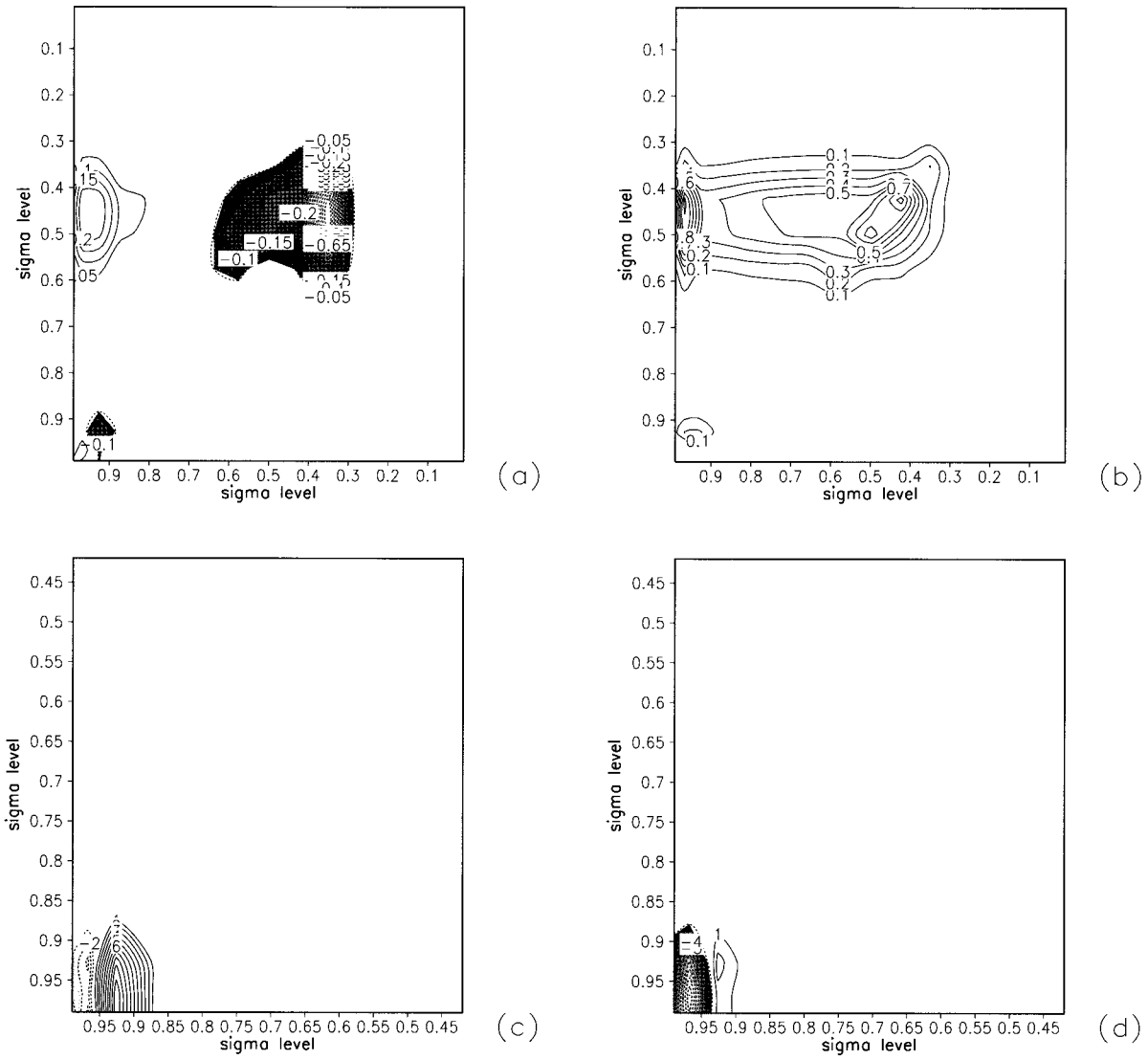

FIG. 6. Same as Fig. 4 but for point (2°S, 25°E): (a) $\nabla_\theta(R_\theta)$, interval 0.05; (b) $\nabla_q(R_\theta)$, interval 0.1; (c) $\nabla_\theta(R_q)$, interval 1.0; and (d) $\nabla_q(R_q)$, interval 1.0.

cause rapid growth of the initial perturbations in the surrounding air.

b. Time-integrated sensitivity

The gradient of the time-integrated response can provide us with an estimate of the influences of initial perturbations on the moisture processes in later time. For this purpose, the matrix **S** in (3) is chosen such that the following two response functions are defined:

$$R_{\theta\theta} = \int_{t_0}^{t_N} \sum_G \left(\frac{\partial\theta}{\partial t}\right)^2 dt$$

$$R_{qq} = \int_{t_0}^{t_N} \sum_G \left(\frac{\partial q}{\partial t}\right)^2 dt. \qquad (15)$$

Here Σ_G represents summation over the globe. These functionals provide a measure of the strength of the impact of convective clouds on the large-scale fields.

The integrations were carried out for 6 h from 0000 to 0600 GMT 1 January 1985. In this section the sensitivity (or gradient) to any variable actually means the sensitivity of the time-integrated response with respect to the perturbation of that variable at initial time.

1) SENSITIVITY TO POTENTIAL TEMPERATURE

Figures 7a and 7b display the longitude–height distribution of $R_{\theta\theta}$ and R_{qq} to θ perturbations, respectively, averaged in the latitudinal band between 10°S and 10°N. A major difference between these two figures and Fig. 3a, which is the instantaneous sensitivity of precipitation

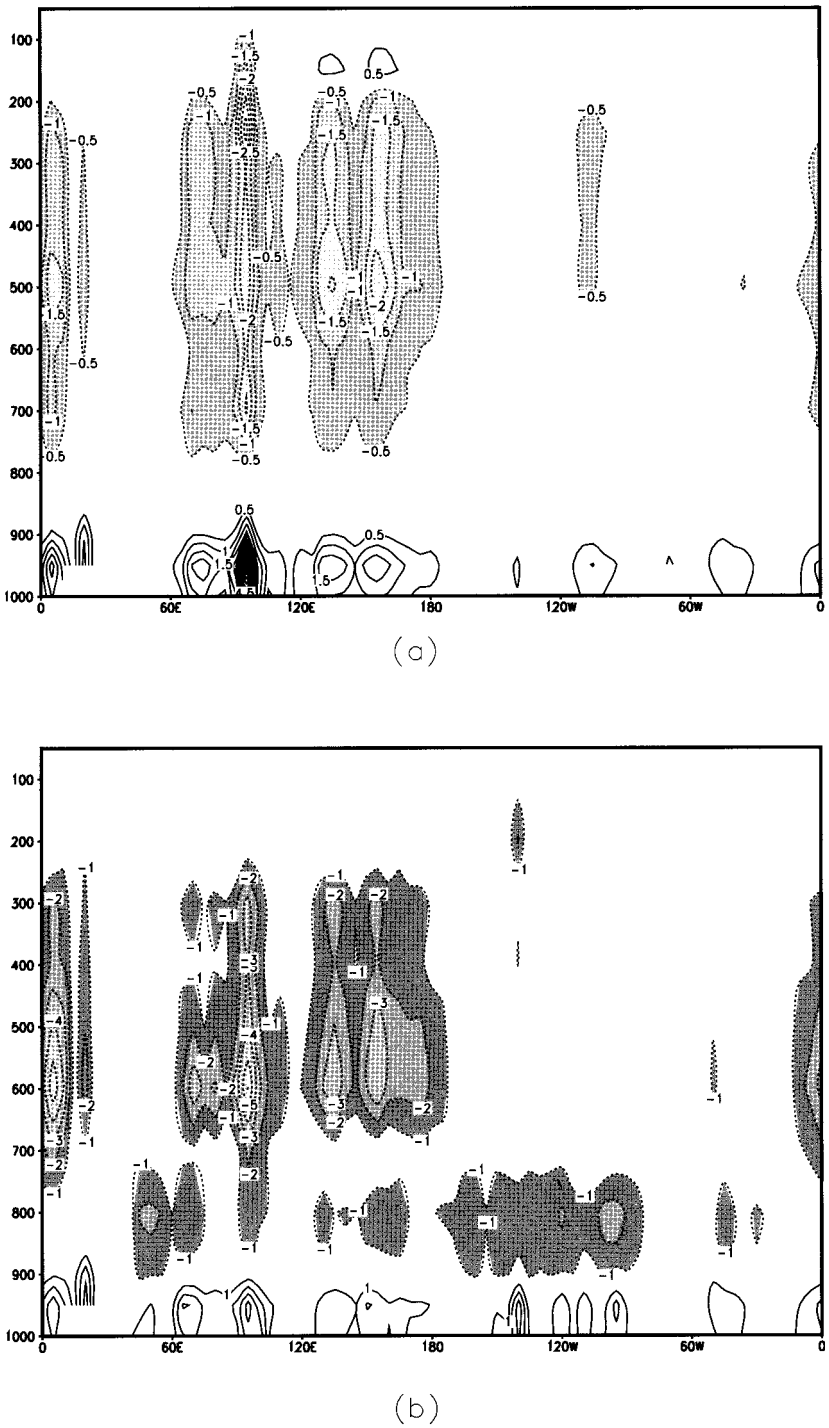

FIG. 7. Variations with longitude and height of the sensitivity to θ perturbations of the response functions: (a) $R_{\theta\theta}$ [interval 0.5, one unit corresponds to 7.2×10^{-7} (K^2 s^{-1}) K^{-1}], and (b) R_{qq} [interval 1.0, one unit corresponds to 1.4×10^{-8} (g $kg^{-1})^2$ s^{-1} K^{-1}], average between 10°S and 10°N. The ordinates are in hPa.

to θ, is that while the latter shows more uniform distribution of negative sensitivity from lower to midtroposphere, in Figs. 7a and 7b significant sensitivity is more concentrated at the 500- and 600-hPa levels, that is, the perturbations occurring at these levels lead to larger variations in $R_{\theta\theta}$ and R_{qq} than similar perturbations at other levels. Specifically, a 1 K increase at subcloud layer or a 1 K decrease around 500 hPa in θ leads to

about 5×10^{-6} K^2 s^{-1} increase and 2×10^{-6} K^2 s^{-1} increase in $R_{\theta\theta}$, respectively.

Figures 7a and 7b also indicate that longitudinally the perturbations over the eastern Indian Ocean and the western Pacific Ocean exert the strongest influence on the convective heating and drying, whereas over the eastern Pacific Ocean, only the temperature perturbations under 800-hPa level can have significant impact.

In summary, the cloud impacts on the large-scale fields are most sensitive to the initial perturbations in the potential temperature field at two levels: one is the subcloud layer, the other is the midtroposphere layer between 500 and 600 hPa. The perturbations at these levels have opposite effects on the convective parameterization, namely, positive perturbations in the lower layers and negative perturbations in the upper layers lead to enhanced convective activities and stronger impact on the environmental fields.

2) Sensitivity to moisture

Figures 8a and 8b show the vertical distribution of the sensitivity to moisture perturbations of $R_{\theta\theta}$ and R_{qq}, respectively, again averaged between 10°S and 10°N. They are quite different from Fig. 3b, which depicts the instantaneous sensitivity of precipitation to the q perturbation. It can be seen from Fig. 8a that $R_{\theta\theta}$ displays a positive sensitivity to all the vertical levels, especially to the levels around 950 and 400 hPa. Specifically, a 1 g kg^{-1} increase in moisture content at 950 hPa (400 hPa) can result in a 1×10^{-5} (1.5×10^{-6}) increase in $R_{\theta\theta}$, which means an increase in convective heating.

Figure 8b, which displays the R_{qq} sensitivity to moisture, shows a somewhat more complex behavior. Only the levels below 300 hPa are displayed since there is very little moisture above this level. The most significant positive gradient is observed around 950 and 600 hPa. From 600 to 500 hPa, the gradient changes from large positive to negative. At around the 600-hPa layer, an addition of 1 g kg^{-1} in the moisture field results in about 2×10^{-7} (g kg^{-1})^2 s^{-1} increase in R_{qq}. On the contrary, adding 1 g kg^{-1} moisture at around 500 hPa tends to suppress convection (cf. Fig. 3b) and reduce the convective drying effect, as manifested by about 1.5×10^{-7}(g kg^{-1})^2 s^{-1} decrease in R_{qq}. This indicates that the moisture process is very sensitive to the vertical profile of the environmental moisture perturbations at midtroposphere level. This intricate structure is also observed in Fig. 4d but with reversed sign since in that figure, the response function is the Δq itself, which is negative, whereas in Fig. 8b the response is the square sum of Δq, which is always positive.

From Fig. 3b it can be seen that the q perturbation around 600 hPa does not significantly influence the strength of convection, which is represented there by convective precipitation, but here we observe that it can very significantly influence the convective drying. A possible explanation is that the convective drying in the environmental air, like the convective heating, is mainly due to the compensating subsidence outside the clouds (Redelsperger and Guichard 1996). This effect is most significant at around 600 hPa (Fig. 1c). Presence of additional moisture in the surrounding air at this level will cause more water vapor to be transported to lower layers by downdrafts, thus leading to a larger depletion of moisture and larger negative Δq, even though the strength of convection does not increase significantly. If, on the other hand, there is additional moisture at higher levels, there is tendency to suppress convective activity so that the cloud-induced drying is reduced accordingly.

While the instantaneous sensitivities account only for the response of RAS to large-scale perturbations, the time-integrated sensitivities incorporate the effect of the interaction between large-scale fields and the RAS scheme through the evolution of the basic field. We compared the instantaneous sensitivity with the time-integrated sensitivity of the same response, either the convective precipitation or the integrands in $R_{\theta\theta}$ and R_{qq}. The differences are not qualitative but only quantitative. For example, Fig. 9 displays the longitude–height distribution of the sensitivity of 6-h integrated convective precipitation to temperature perturbations, also averaged between 10°S and 10°N. Comparing it with the instantaneous sensitivity of Fig. 3a, one can see that the general patterns are quite similar but the positive centers at 950 hPa and negative centers around 500 hPa are enhanced in the time-integrated sensitivity, which accounts for the larger vertical variation in Fig. 9 than in Fig. 3a. The conclusion is generally valid for other response functions.

3) Sensitivity to the wind field

The wind fields do not exert an immediate impact on the RAS scheme, so there is no instantaneous sensitivity to wind field. However, the wind field redistributes θ and q perturbations through advection and convergence/divergence. In this way it provides an indirect influence on the output of the RAS scheme. The integration of the adjoint model can provide us with the gradient of $R_{\theta\theta}$ and R_{qq} from RAS with respect to the wind field.

The vertical distribution of the gradient to zonal (u) and meridional (v) components of the wind field (figures omitted) both show a significant baroclinic structure with a vertical profile very similar to that of standing wavenumber 1. The node is at 500 hPa, with opposite signs below and above it. But within each regime, the structure exhibits a barotropic behavior. The two most influential levels are located near 750 and 300 hPa, respectively.

By displaying the gradient of $R_{\theta\theta}$ with respect to u and v components in vector form, we obtain a concise view of the sensitivity to the perturbations in the wind vector. Figures 10a and 10b show the horizontal distribution of the sensitivity of $R_{\theta\theta}$ to the wind vector at 200 and 700 hPa, which represents the situation at the upper

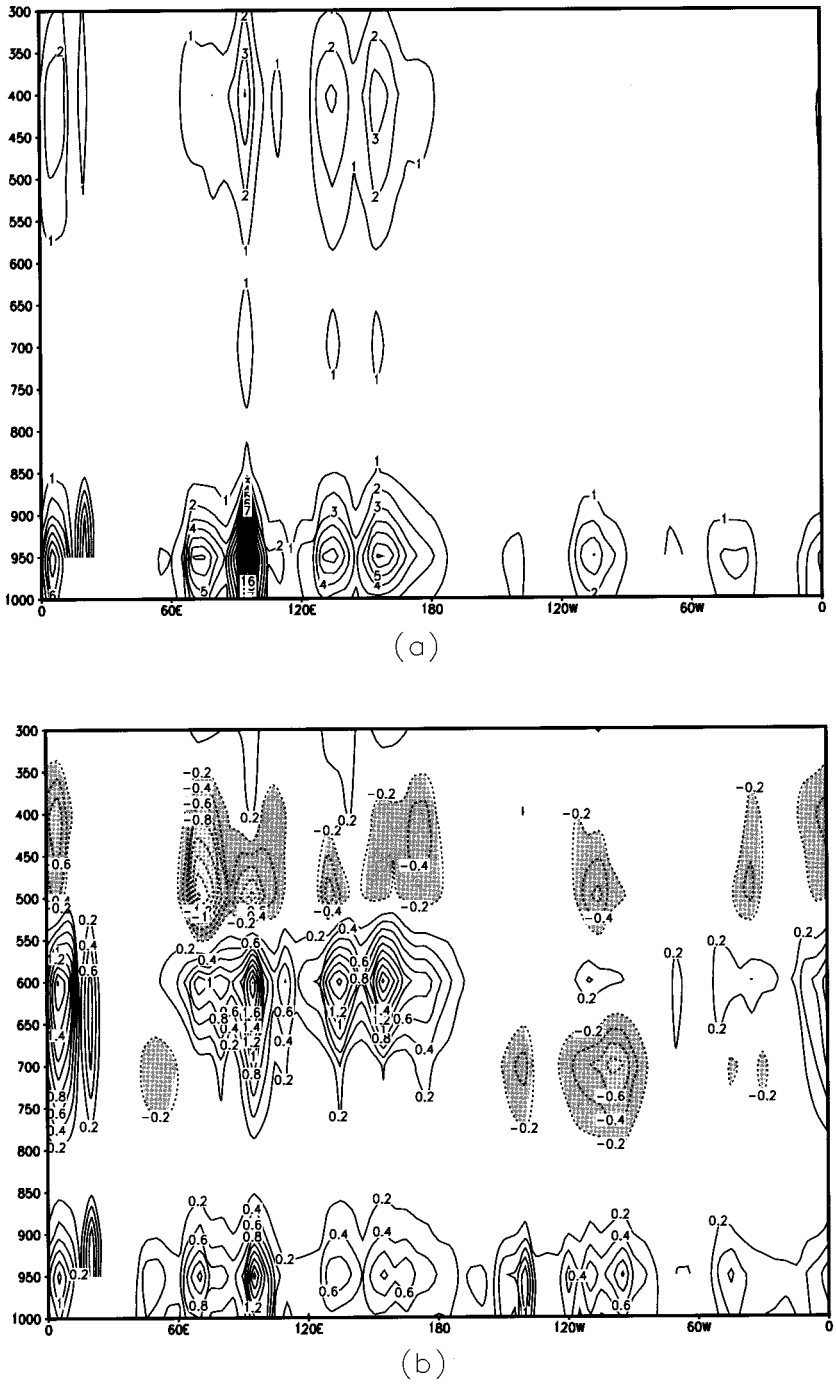

FIG. 8. Height–longitude distribution of sensitivity to moisture perturbations of the response functions: (a) $R_{\theta\theta}$ [contour interval 1.0, one unit corresponds to 5.18×10^{-7} (K^2 s^{-1}) (g kg^{-1})$^{-1}$], and (b) R_{qq} [interval 0.2, one unit corresponds to 1.0×10^{-7} (g kg^{-1})^2 s^{-1} (g kg^{-1})$^{-1}$], average between 10°S and 10°N. The ordinates are in hPa.

and lower levels, respectively. The gradients of $R_{\theta\theta}$ at the two aforementioned layers have opposite signs, again indicating a baroclinic character. The most significant influence is due to the divergent component, whereas the vorticity component is very weak except at some isolated areas at high latitudes. The lower (upper) level gradient vector is largely convergent (divergent). The sensitivity to wind of R_{qq} is very similar to that of $R_{\theta\theta}$ and therefore is not shown here. As discussed in section 2, wind perturbations with the same structure

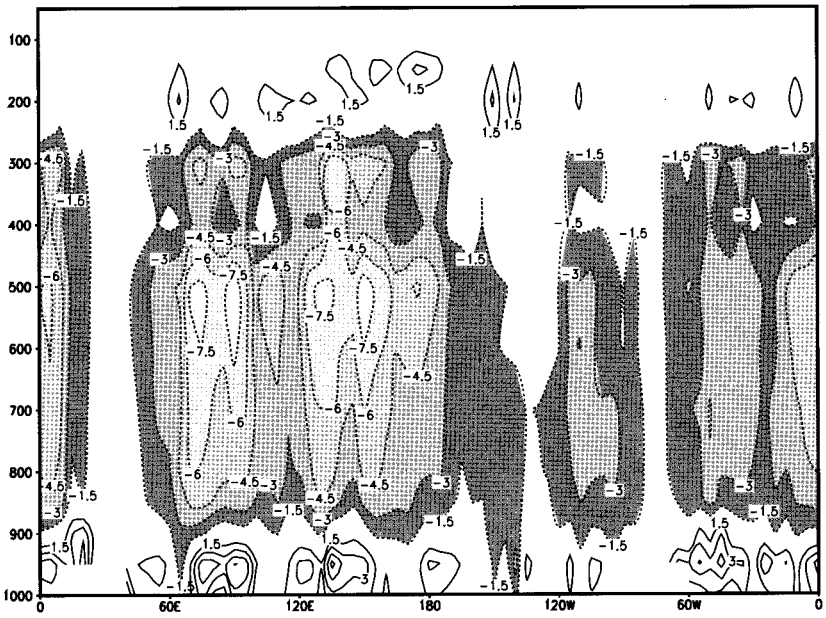

FIG. 9. Longitude–vertical distribution of the sensitivity of the 6-h integrated RAS precipitation to perturbations in the potential temperature field, averaged between 10°S and 10°N [interval 1.5, one unit corresponds to 1.4 (mm day^{-1}) K^{-1}]. The ordinate is in hPa.

and distribution, that is, convergence at lower levels and divergence at upper levels over the convectively active regions at initial time, will lead to stronger cloud impacts on the environment in the ensuing several hours. The most sensitive region extends geographically from the eastern Indian Ocean to the western Pacific Ocean at low latitudes.

c. Relative sensitivity of different variables

In the above we investigated the impacts of the perturbations in potential temperature, moisture, and wind fields on the response functions. To provide a quantitative idea of the relative importance of each of these fields in causing the variation in the response functions, here we carry out a comparison contained in Table 1.

Considering their natural variability and typical observational error, the disturbances in the above fields are prescribed as shown in the first column of Table 1. Let us further suppose that each of these perturbations occurs at the most sensitive grid point for that variable (i.e., the point with the largest gradient). Table 1 lists the variations in the three response functionals resulting from each individual perturbation. It can be seen that for the precipitation (δR_p), θ is the most influential factor. Its impact is about 2.5 times that arising from q perturbations. For convective heating and drying, the q perturbation becomes the most influential factor although θ perturbation is almost as important. The variation caused by the wind perturbations is at least one order of magnitude smaller than that due to the θ and q perturbations, respectively.

When examining Table 1, one should bear in mind that the magnitude of perturbations here is somewhat outside the range of validity of linear approximation as indicated in Fig. 2, although the discrepancy is very small. Note that a 1 K change in θ is not so unusual since it is well within the range of analysis errors of present assimilation systems. Such a perturbation can cause a variation as large as 10 mm day^{-1} in convective precipitation locally. Although this result is only for a particular case, it does suggest a high sensitivity of the moisture scheme to perturbations (or analysis errors) in large-scale fields. This large sensitivity is also observed in Fig. 3.

As a side note we remark that a study on the climatology of the parameterized physical processes in the GEOS-1 GCM and GEOS-1 DAS indicates biases in the GCM climate with respect to observed climate. Among these are (a) a much too wet upper troposphere (300 mb) over the Pacific Ocean and (b) the Tropics and Subtropics over the oceans are too dry when compared with the vertically integrated moisture from Special Sensor Microwave/Imager (SSM/I) measurements. This latter is caused by excessive precipitation (moisture sink) at the early stage of model integration and

TABLE 1. First-order variations in the response functionals.

		δR_p (mm day^{-1})	$\delta R_{\theta\theta}$ (K^2 s^{-1})	δR_{qq} (g^2 kg^{-2} s^{-1})
$\delta\theta$	1 K	10.0	1.4×10^{-5}	2.2×10^{-7}
δq	1 g kg^{-1}	4.0	2.9×10^{-5}	5.0×10^{-7}
δW	1 m s^{-1}		1.5×10^{-8}	1.0×10^{-8}

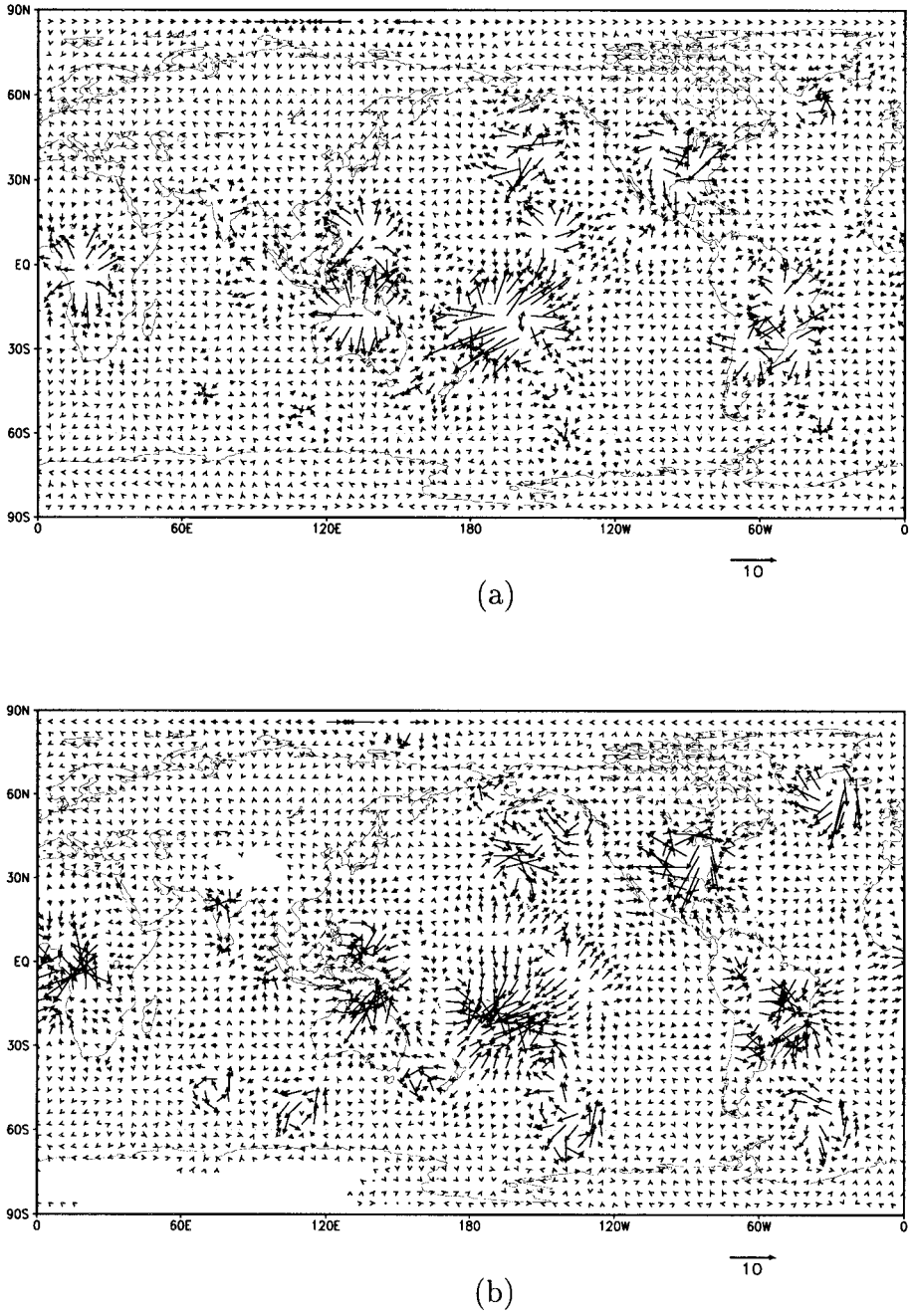

FIG. 10. Sensitivity of $R_{\theta\theta}$ response to perturbations in wind vector at (a) 200 hPa and (b) 700 hPa. One unit length of vector corresponds to 5.2×10^{-10} (K^2 s^{-1}) (m s^{-1})$^{-1}$.

overadjustment of the tropical atmosphere by convective parameterization in the GCM (Molod et al. 1996). Our result suggests that lower (higher) temperature at the subcloud (midtroposphere) layers and less moisture content at the lower troposphere at initial time may suppress convective precipitation and therefore may alleviate the initial precipitation spinup from the RAS scheme.

d. The impact of large-scale condensation and reevaporation

In the above experiments, the RAS scheme, supersaturation, or large-scale condensation and reevaporation are all included in both the forward and adjoint model. Here, to evaluate the effect of the latter two processes on sensitivity, we repeated the above experiments with the effects of large-scale rainfall and reevap-

FIG. 11. Height–longitude distribution of sensitivity of the response function R_{qq} to perturbations in (a) the potential temperature field [contour interval 1.0, one unit corresponds to 1.4×10^{-8} (g kg^{-1})^2 s^{-1} K^{-1}], and (b) the moisture field (interval 0.2, one unit corresponds to 1.0×10^{-7} (g kg^{-1})^2 s^{-1} (g kg^{-1})$^{-1}$] without large-scale moisture processes, averaged between 10°S and 10°N. The ordinates are in hPa.

oration turned off in the adjoint model. For simplicity, these two processes are hereafter referred to as large-scale moisture processes.

Figure 11a shows the sensitivity of R_{qq} response to θ without large-scale moisture processes. Comparing with Fig. 7b one observes that the strongest negative sensitivity center at around 600 hPa disappears in Fig. 11a, which means that with large-scale moisture processes the moist model is more sensitive to environmental θ perturbation. Figure 11b shows the sensitivity of R_{qq} to

moisture in the absence of large-scale processes. A comparison with Fig. 8b indicates that with large-scale processes, the positive sensitivity to moisture perturbations at around 600 hPa is strengthened, although the general structure of the distribution of sensitivity is unchanged.

Since the sensitivity is analyzed here in the linear regime, the explanation is relatively simple. On one hand, negative θ and positive moisture perturbations at midtroposphere mean that the gridscale condensation is more likely to happen, leading to larger negative $\partial q/\partial t$ and larger R_{qq}. On the other hand, from Figs. 11a and 11b, negative θ and positive moisture perturbations around 600 hPa induce stronger convective activities, meaning that more moisture is transported upward, which favors large-scale condensation at midtroposphere, thus leading to larger R_{qq}. Therefore the gradient of the R_{qq} to temperature and moisture perturbations around 600 hPa is enhanced by taking large-scale moisture processes into account.

For the sensitivity of the $R_{\theta\theta}$ response to moisture without large-scale moisture processes (figure not shown), the major difference from Fig. 8a is the disappearance of large positive sensitivity around 400 hPa. This means that with large-scale moisture processes, positive moisture perturbations at midtroposphere tend to induce a larger $\partial\theta/\partial t$. This occurs since more moisture at midtroposphere level favors large-scale condensation, and the condensational latent heating process produces larger temperature variation. The lower troposphere is virtually not affected by the large-scale moisture processes. The impact of large-scale moisture processes on the sensitivity of $R_{\theta\theta}$ to temperature perturbation is very small.

Generally speaking, the effect of large-scale moisture processes is significant at the midtropospheric level and it enhances the model sensitivity to perturbations in θ and moisture. Of course in the nonlinear GCM, a complicated interaction occurs between the RAS scheme and large-scale processes and sometimes they are not fully distinguishable. Therefore this issue cannot be fully addressed here in the framework of the adjoint model. We can obtain only a general idea of the contribution to sensitivity of each of the processes.

5. Summary and conclusions

Sensitivity of the RAS scheme used in NASA's GEOS-1 GCM to perturbations in large-scale environmental fields was analyzed using the adjoint of the RAS parameterization scheme and the GCM. The integrations of the adjoint model yield the gradients of the response functionals, which are measures of the strength of the cloud precipitation, the convective heating and convective drying effects, respectively, with respect to perturbations of large-scale environmental fields. The most sensitive (in terms of the response functions) and the most influential (in terms of the large-scale perturbations) vertical levels were identified and the relative importance of the different variables was evaluated.

The results obtained show that the potential temperature perturbation has a significant impact on all the response functionals analyzed, especially on the convective precipitation. The perturbations at subcloud layers and at midtroposphere, from 500 to 600 hPa, are found to be the most influential. The effects from lower layers and upper layers are opposite to each other, that is, positive (negative) temperature perturbations at lower (upper) levels tend to produce positive variations to the response functions, indicating stronger convectivities and stronger cloud impact on the surrounding air.

The impact from moisture field is most significant on the cloud heating and drying effects and the strongest influence comes from the subcloud layers, where additional moisture is conducive to stronger convective activities. The cloud-induced drying (moistening) can also be significantly influenced by the moisture perturbations at midtroposphere, with completely opposite effects from perturbations occurring at 500 hPa as compared to the corresponding ones at 600 hPa, indicating a strong sensitivity of the response to gridscale vertical profiles at midtroposphere.

The regions where the perturbations are most effective in inducing variations in the response functions extends geographically from the eastern Indian Ocean to the western Pacific Ocean at low latitudes, where the convective activities are intense and frequent in a climatological sense.

The effects of the perturbations on convection are interpreted in terms of stability in the subcloud levels and the buoyancy force supporting cloud activities as well as the vertical heat/moisture transport by convection.

The implications of these sensitivity analysis results are that accurate data of temperature, moisture, and surface pressure are essential for an accurate evaluation of the cumulus cloud effects, especially at the most influential vertical levels, which were identified above, since small perturbations at these locations tend to exert a stronger influence on the RAS outputs than the same perturbations at other locations.

One has to be very careful in comparing the sensitivity at different vertical levels, especially the sensitivity to moisture, due to the large variability in mean moisture content at different levels. The sensitivity analysis only tells us in which area the perturbation can cause a larger variation in the response function, in case that the same perturbation occurs everywhere. But the actual change depends on how the real perturbation is distributed. Although from Figs. 8a and 8b we see that the gradient of the response to moisture at higher levels (from 600 to 400 hPa) is of about the same magnitude as that at lower levels (around cloudbase level), it does not mean that they exert the same influence on the response function. We expect the impact from lower levels to be much stronger due to the larger mean humidity

and larger variability. However, it is also probable that the actual variation of high-level moisture in a convective area is much larger than its normal large-scale variability at the same level. In this case it may exert a significant impact on the response function.

The Jacobian of the cloud-induced $\Delta\theta$ and Δq to θ and q perturbations in a single air column, besides identifying the vertical levels of most sensitive response and most influential perturbations at various geographical locations, indicates the feedback between cloud activities and gridscale perturbations in the surrounding air. It shows that the cloud-induced heating and drying at levels between 400 and 600 hPa feel the strongest impact from perturbations in large-scale fields. Most of the vertical layers show negative feedback between convective heating and potential temperature perturbations and between convective drying and moisture perturbations in the environment. However, there are also some vertical layers in the midtroposphere where the feedback is positive, indicating that the initial small perturbations can amplify through cloud effects. Therefore, the above results should help to focus attention on data quality at those levels and areas with positive feedback.

The influence due to perturbations in the wind field is normally weaker than that due to perturbations in θ and q fields, but a reasonable sensitivity pattern was still obtained, namely, convergence (divergence) at lower (upper) layers is favorable to convective activities and leads to a stronger cloud impact.

The impact of large-scale condensation and reevaporation on the sensitivity is also analyzed in the linear regime. Their effect is significant at the midtropospheric level and they enhance the model sensitivity to perturbations in temperature and moisture fields.

The results from the present work may have important bearings on variational data assimilation, particularly the assimilation of precipitation data, in which moist convection is the dominant process. In a 3D variational assimilation of the precipitation data, the difference between model output rainfall and the observed rainfall (or the derivative of the cost function) is taken as input to the adjoint RAS scheme, and the output is the gradient of this cost function with respect to the large-scale variables. We may expect that the most influential levels identified in the present work are the ones most responsible for the reduction of the misfit, or the forecast error, which is represented by the cost function. In other words, these levels are the ones expected to experience the largest impact from observational data. This information can also be applied to the investigation of where additional adaptive observations should be taken.

We may expect that availability of better initial data in these sensitive areas and levels can also improve model ''precipitation spinup'' during the first few hours of a numerical forecast. We intend to pursue this topic in future research. Moreover, we are in the process of carrying out an adjoint sensitivity analysis of the moisture parameterization to some model parameters in order to provide us with some clues on ranking the most important parameters in the RAS package aiming at conducting optimal parameter estimation combined with 4D variational data assimilation.

Acknowledgments. The first and second authors acknowledge support by NASA Grant NAG 5-1660 managed by Dr. Ken Bergman, section head of Climate Modeling, NASA headquarters. Thanks are due to Dr. Zhijin Li from the Supercomputer Research Institute (SCRI) at The Florida State University for many fruitful discussions during the research. We also thank an anonymous reviewer and Dr. Y. C. Sud for their comments and suggestions, which helped us much to improve the manuscript. The data used in this work were obtained from the archived dataset in DAO/NASA. All the computations were carried out on NASA's CRAY J90. This research was also supported by Supercomputer Computations Research Institute at The Florida State University, which is partially funded through Contract DE-FC0583ER250000.

REFERENCES

Cacuci, D. G., 1981a: Sensitivity theory for nonlinear systems. Part I: Nonlinear functional analysis approach. *J. Math. Phys.,* **22,** 2794–2802.

——, 1981b: Sensitivity theory for nonlinear systems. Part II: Extensions to additional classes of responses. *J. Math. Phys.,* **22,** 2803–2812.

——, 1988: The forward and adjoint methods of sensitivity analysis. *Uncertainty Analysis,* Y. Ronen, Ed., CRC Press, 71–144.

Fillion, L., and R. Errico, 1997: Variational assimilation of precipitation data using moist convective parameterization schemes: A 1D-var study. *Mon. Wea. Rev.,* **125,** 2917–2942.

Hall, M. C. G., 1986: Application of adjoint sensitivity theory to an atmospheric general circulation model. *J. Atmos. Sci.,* **43,** 2644–2651.

——, D. G. Cacuci, and M. R. Schlesinger, 1982: Sensitivity analysis of a radiative-convective model by the adjoint method. *J. Atmos. Sci.,* **39,** 2038–2050.

Molod, A., H. M. Helfand, and L. L. Takacs, 1996: The climatology of parameterized physical processes in the GEOS-1 GCM and their impact on the GEOS-1 Data Assimilation System. *J. Climate,* **9,** 764–785.

Moorthi, S., and M. J. Suarez, 1992: Relaxed Arakawa–Schubert: A parameterization of moist convection for general circulation models. *Mon. Wea. Rev.,* **120,** 978–1002.

Navon, I. M., 1998: Practical and theoretical aspects of adjoint parameter estimation and identifiability in meteorology and oceanography. *Dyn. Atmos. Oceans,* **27,** 55–79.

Rabier, F., P. Courtier, and O. Talagrand, 1992: An application of adjoint models to sensitivity analysis. *Beitr. Phys. Atmos.,* **65,** 177–192.

——, E. Klinker, P. Courtier, and A. Hollingsworth, 1996: Sensitivity of forecast errors to initial conditions. *Quart. J. Roy. Meteor. Soc.,* **122,** 121–150.

Redelsperger, J. L., and F. Guichard, 1996: Detailed analysis of cloud systems observed during TOGA-COARE: Simulations forced and unforced by the large scale motions. *Proc. ECMWF Workshop, New Insights and Approaches to Convective Parametrization,* Reading, United Kingdom, ECMWF, 58–76.

Rinne, J., and H. Järvinnen, 1993: Estimation of the Cressman term for a barotropic model through optimization with the use of the adjoint model. *Mon. Wea. Rev.,* **121,** 826–833.

Schubert, S. D., J. Pfaendtner, and R. B. Rood, 1993: An assimilated data set for Earth science applications. *Bull. Amer. Meteor. Soc.*, **74,** 2331–2342.

Sud, Y. C., and A. Molod, 1988: The roles of dry convection, cloud-radiation feedback processes and the influence of recent improvements in the parameterization of convection in the GLA GCM. *Mon. Wea. Rev.*, **116,** 2366–2387.

Takacs, L. L., A. Molod, and T. Wang, 1994: Documentation of the Goddard Earth Observing System (GEOS) general circulation model—Version 1. NASA Tech. Memo. 104606, Vol. 1, 64 pp.

Yang, W., and I. M. Navon, 1996: Documentation of the tangent linear model and its adjoint of the adiabatic version of the NASA GEOS-1 C-grid GCM—Version 5.2. NASA Tech. Memo. 104606, Vol. 8, 61 pp.

——, ——, and R. Todling, 1997: Documentation of the tangent linear and adjoint models of the Relaxed Arakawa–Schubert moisture parameterization packages of the NASA GEOS-1 GCM—Version 5.2. NASA Tech. Memo. 104606, Vol. 11, 40 pp.

Zou, X., A. Barcilon, I. M. Navon, J. Whitaker, and D. G. Cacuci, 1993: An adjoint sensitivity study of blocking in a two-layer isentropic model. *Mon. Wea. Rev.*, **121,** 2833–2857.